

Quantifying Viral Propagation in Vitro: Toward a Method for Characterization of Complex Phenotypes

Karen A. Duca,^{†,||} Vy Lam,[†] Iris Keren,^{†,⊥} Elizabeth E. Endler,[†]
Geoffrey J. Letchworth,[§] Isabel S. Novella,[‡] and John Yin^{*,†}

Department of Chemical Engineering, University of Wisconsin, Madison, Wisconsin, Department of Microbiology and Immunology, Medical College of Ohio, Toledo, Ohio, and USDA, ARS, ABADRL, Laramie, Wyoming

For a eukaryotic virus to successfully infect and propagate in cultured cells several events must occur: the virion must identify and bind to its cellular receptor, become internalized, uncoat, synthesize viral proteins, replicate its genome, assemble progeny virions, and exit the host cell. While these events are taking place, intrinsic host defenses activate in order to defeat the virus, e.g., activation of the interferon system, induction of apoptosis, and attempted elicitation of immune responses via chemokine and cytokine production. As a first step in developing an imaging methodology to facilitate direct observation of such complex host/virus dynamics, we have designed an immunofluorescence-based system that extends the traditional plaque assay, permitting simultaneous quantification of the rate of viral spread, as indicated by the presence of a labeled viral protein, and cell death in vitro, as indicated by cell loss. We propose that our propagation and cell death profiles serve as phenotypic readouts, complementing genetic analysis of viral strains. As our virus/host system we used vesicular stomatitis virus (VSV) propagating in hamster kidney epithelial (BHK-21) and murine astrocytoma (DBT) cell lines. Viral propagation and death profiles were strikingly different in these two cell lines, displaying both very different initial titer and cell age effects. The rate of viral spread and cell death tracked reliably in both cell lines. In BHK-21 cells, the rate of viral propagation, as well as maximal spread, was relatively insensitive to initial titer and was roughly linear over several days. In contrast, viral plaque expansion in DBT cells was contained early in the infections with high titers, while low titer infections spread in a manner similar to the BHK-21 cells. The effect of cell age on infection spread was negligible in BHK-21 cells but not in DBTs. Neither of these effects was clearly observed by plaque assay.

Introduction

The complete sequencing of genomes from a range of organisms is generating data at a rate unprecedented in the history of biology (1, 2). Moreover, the dual techniques of gene and protein expression profiling are identifying important players on the stage during any given window of development or disease etiology, as well as how the levels of these components fluctuate over time or in response to environmental changes (3–6). The need to move from component expression level readouts to actual in situ observation of the complex biochemical phenotypes emerging from the underlying genetic variation is becoming increasingly important. In this paper we present the first step in the development of an imaging methodology that will ultimately permit quantification of the phenotypic outcome of genetic variability in eukaryotic viruses in terms of a broad range of detectable biochemical events

associated with infection in vitro, e.g., rate of viral spread from cell to cell; apoptosis or stress response induction; chemokine/cytokine synthesis; interferon-mediated viral replication shutdown; viral transcription, translation, and replication; as well as association of viral messages and proteins with various host compartments. Eventually, we expect that our system can be tailored to monitor a wide array of virus/host systems and specific interactions.

Historically, the plaque assay, in addition to providing a metric of infectious titer, has been a valuable virological tool to qualitatively assess an important characteristic of a given virus, viz., replicative ability (7–15). The sizes of areas of cell destruction or syncytium formation, designated as small, medium, and large plaques, reflect the virus' propensity to infect and spread in cell culture. This is often correlated with the ability of a virus to spread in an intact animal and has been used frequently to select small plaque viruses for vaccine use. Plaques are generally observed at one defined time point post-infection, although several groups have also measured diameters of populations of plaques at several time points postinfection (16–18). This assay is simple to perform and straightforward to interpret, but it provides no mechanistic information and must be modified to include immunostaining for viruses that are not strongly cyto-

* Ph: (608) 265-3779. Fax: (608) 262-5434. E-mail: yin@engr.wisc.edu.

† University of Wisconsin.

‡ Medical College of Ohio.

§ USDA.

|| Present address: Department of Electrical Engineering and Computer Science, Tufts University, Medford, MA.

⊥ Present address: Department of Microbiology and Immunology, Medical College of Ohio, Toledo, OH.

lytic. Moreover, we show here that the plaque assay can actually mask information about the nature of viral spread.

This study represents our first step toward the development of an imaging method that is capable of viewing "whole system" host/virus behavior and mapping it to underlying genetic variation in either the virus or host. The model system employed was vesicular stomatitis virus, (VSV-Indiana), a nonfatal vesiculating disease of cattle and horses (19). VSV has long been used as a model system for studying viral replication because of its high infectivity and ability to grow to high titer in cell culture (20, 21). As susceptible hosts, we used two different cell types, both of which are naturally infectable by VSV, an epithelial cell line (BHK-21, baby hamster kidney) and a murine astrocytoma (DBT, delayed brain tumor). By means of indirect immunofluorescence and nuclear staining, we visualized infected cells, which reached well beyond the area of cell destruction normally associated with plaques, thereby extending the usefulness of the standard assay. We located and measured the areas of cell destruction relative to the advancing viral front to estimate the approximate time between the first appearance of infection and cell death.

In this report, we introduce the concept of an "event front marker" that has a propagation profile in any given virus/host system as a quantifiable phenotype that may serve as a useful identifier *in vitro*. This study presents propagation profile data from two events (infection and cell death) and examines the effect of experimental parameters on these profiles. The nature of viral spread and cell destruction in the two cell types is quite different. From this study it was also clear that the assay may be further extended to include cell-based antiviral responses that are responsible for the observed propagation differences. We hope that our method may also find applications as (1) a prescreening system for novel antiviral therapeutics targeting any phase of the viral life cycle; (2) a reporter system for synergistic cytopathological effects arising from virus–drug interactions; and (3) a fundamental kinetic probe of the complex dynamics of virus/host and infected/uninfected cell interactions for eventual *in silico* simulations.

Materials and Methods

Cell Culture. Baby hamster kidney cells (BHK-21) were grown as monolayers at 36.50 °C in a humidified, 5% CO₂ atmosphere. Growth medium consisted of Minimal Essential Medium with Earle's salts (Gibco BRL), 10% fetal bovine serum (FBS, Hyclone), and 2 mM glutamine (Glutamax I, Gibco BRL). Cells were passaged approximately every fourth day. For subculture, monolayers were rinsed with Hanks Balanced Salt Solution, incubated in 0.05% trypsin/53 mM EDTA (Fisher) for 6–7 min and replated in fresh growth medium at a 1:10 or 1:20 dilution. Murine delayed brain tumor (DBT) cells were obtained from J. Fleming (University of Wisconsin) and grown under the same temperature and atmospheric conditions. Growth medium included Dulbecco's Modified Eagle Medium (Gibco BRL), 10% newborn calf serum (NCS, Hyclone), 2 mM Glutamax I, and 7.5 mM HEPES (Sigma). Passage conditions were identical to the BHK-21 cells with the exception that 0.025% trypsin/25 mM EDTA was used to remove cells. No antibiotics were used with either cell line, and cells were passed no more than 3 months to eliminate artifacts due to cell senescence. Viability at the time of experiments always approached 100%.

Focal Infection of Tissue Culture Monolayers. Cells were harvested, resuspended in growth medium, and placed into six-well plates at a concentration of 5×10^5 cells/well in 2-mL volumes. Plates were returned to the incubator for 12–24 h. Cells were then rinsed once in infection medium (standard culture medium with 2% FBS) in preparation for the overlay.

The quality and consistency of the agarose overlay are critical for this assay. We tested several agarose types (high vs low melting, variable purity grades) from three vendors. All agarose lots were successful, but each required a different percentage of agarose to achieve a rigid overlay without microchannels between the cells and the agarose. In addition, agarose aging resulted in a firmer overlay at lower concentration. A 0.6 wt %/vol agarose overlay was chosen for this series of experiments. Ultrahigh purity, high melting point agarose (Biorad) was hydrated with nanopure water (approximately 10% of the desired final volume) and sterilized by autoclaving at 121 °C for 20 min. The sterile agarose solution was combined with infection medium (at 42–45 °C) to make the overlay mixture. Overlay was also prepared by diluting the agarose in 50% of the final desired volume of H₂O and mixing with prewarmed 2× infection medium. This method did not produce different results from the first. Medium was suctioned from the wells, and 4 mL of overlay was carefully added. Plates were then rocked and swirled gently to mix the surface layer of medium with the warm overlay. Plates were left at room temperature in the dark for 15–20 min to solidify. They were then returned to the incubator for at least 30 min equilibration before infection.

A small virus deposition reservoir ($r = 1$ mm) was made by punching a hole in the center of each well with a Pasteur pipet. (See Figure 1A.) A small plug of overlay was removed by applying gentle manual suction through the pipet. A concentrated stock of vesicular stomatitis virus (VSV-Indiana serotype, Mudd-Summers strain) in cell culture supernatant at 5×10^9 pfu/mL was serially diluted in infection medium to the desired concentrations. Each well received 5 μ L of virus solution; there was no overflow from the well. The infected plates were carefully returned to the incubator to avoid splashing virus out of the reservoir. Plates remained in the incubator until the times designated for fixation.

Plaque Assays. Cells were plated at a density of 5×10^5 cells/well in six-well plates 1 day before infecting. Monolayers were rinsed with infection medium, overlaid with 200 μ L of viral suspension, and returned to the incubator. Half of the wells received an inoculum of 10 pfu, while the other half received 25 pfu. The virus was incubated on the cells for 45 min with gentle rocking every 15 min and subsequently removed. The cells were rinsed with Hanks Balanced Salt Solution (HBSS, Fisher). Monolayers were then overlaid with 4 mL of 0.6% agarose diluted in infection medium as described above. Plates were fixed in formalin (Fisher) at 24, 36, and 48 h postinfection. After removal of the overlay, the fixed monolayers were rinsed twice with 10 mM phosphate buffered saline (PBS, Sigma) and stained with 0.5% Gentian violet (Sigma) to visualize plaques. Plaque diameters were measured with a millimeter ruler.

Fixation and Immunocytochemistry. Monolayers were fixed at room temperature at selected time points up to several days postinfection. The fixative consisted of 4% paraformaldehyde (w/v) and 5% sucrose (w/v) in 10 mM PBS, pH 7.2. After 2–3 h, the agarose overlay was removed and the cell monolayers washed twice for

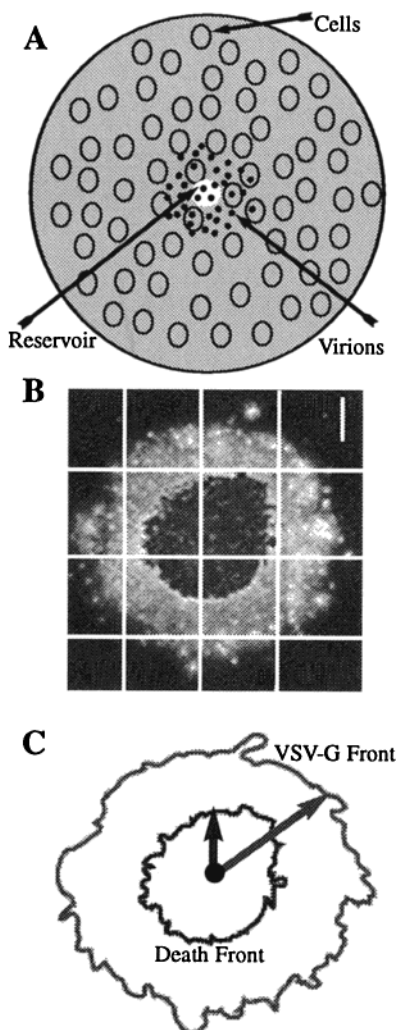


Figure 1. The event front marker assay comprised focal infection of a cell monolayer, multiple image collection, and area equivalent radius (AER) calculation. A small hole was punched into the center of a cell monolayer overlaid with 0.6% agarose into which virus was deposited. The infection began in the reservoir and propagated outward radially (panel A). At specified times, multiple monolayers were fixed and stained for the presence of VSV-G protein to visualize viral infection. Nuclei were labeled with DAPI to visualize the absence of intact cell nuclei, an indicator of cell death. The entire infected area was sequentially scanned at $4\times$ magnification using an x - y translation stage. The composite image was then montaged, bar = 1 mm. (panel B) The infected area in the micrograph was manually outlined, as well as the area of cell death. Both areas were then approximated as circles, and a radius was calculated for each, i.e., an area equivalent radius (AER). The average AER from replicate wells was calculated and plotted as a function of time to obtain an event front profile. Taken together, all the profiles served as a phenotypic fingerprint for the particular host/virus combination with respect to the events that the markers represent. (Panel C) In this first study we examined the infection front and the cell death front.

10 min each in PBS. The plates were stored in PBS containing 0.01% NaN_3 (Sigma) at 4°C until staining.

The distribution of virus was visualized by indirect immunofluorescence of VSV-G protein. Monolayers were washed once with 2 mL of PBS/5% normal serum and once with 2 mL PBS/5% normal serum/0.1% saponin; each wash lasted 10 min at room temperature. Cells were then blocked for 20 min with 1 mL of PBS/5% normal serum/0.2% bovine serum albumin (BSA)/0.1% saponin. A monoclonal antibody against VSV-G (IL-2) (22) was obtained as murine ascites fluid from P. Mathews (NKI/

NYU). The primary antibody was diluted 1:500 in PBS/5% normal serum/0.1% saponin, and 0.5 mL was added to each well. Plates were incubated with the antibody overnight at 4°C . The following day cells were washed twice with PBS/0.1% saponin and once with PBS/5% normal serum/0.1% saponin and blocked with PBS/0.2% BSA/5% normal serum/0.1% saponin as before. A Cy3-conjugated donkey anti-mouse $\text{F}(\text{ab}')_2$ secondary antibody (Jackson ImmunoResearch) was diluted 1:300 in PBS/0.1% saponin. Monolayers were incubated in the dark for 50–60 min at room temperature in 0.5 mL of secondary antibody solution. After incubation, cells were washed twice with PBS/0.1% saponin to remove unbound antibody. To visualize nuclei, wells were incubated with $0.3\ \mu\text{M}$ DAPI (4',6-diamidino-2-phenylindole) for 5 min and rinsed three times with PBS. Plates were stored at 4°C in PBS/0.01% NaN_3 prior to imaging. Both primary and secondary antibodies were well characterized for specificity; neither primary nor secondary antibody used alone resulted in any fluorescent signal.

Image Collection, Processing, and Analysis. Images were acquired using a Nikon TE300 inverted epifluorescent microscope equipped with a Prior x - y translation stage. A monochrome SensSys 4.0 cooled CCD camera driven by Metamorph 4.0 software. (Universal Imaging) running on a Pentium II (Windows 95) captured digital images of the infected monolayers. The location and extent of infection was identified in each well, and the number of microscope fields necessary to fully image the infected area at $4\times$ magnification was estimated (1–100 fields). The system was then programmed to move the stage consecutively across the entire infected area, acquire an image at each location, and finally, seamlessly combine the individual images into a single montage (see Figure 1B). The Cy-3 and DAPI channels were probed sequentially. In some cases, the images were then pseudocolored red and blue, respectively, and superimposed.

Prior to analysis, images were preprocessed to enhance contrast and resized to be easily accommodated on a computer screen using Adobe Photoshop 5.0.2 running on an Apple G3 (Mac OS 8.x). Analysis was done with Scion Image v1.62a. The infected area was determined by the presence of the labeled VSV-G protein and manually outlined. Only contiguous areas were included in the calculations; satellites outside the infected area were infrequent and excluded. The area of cell death, as indicated by absence of nuclei (corresponding to the plaque), was also outlined (see Figure 1C). This second measurement was more difficult, as cell death was not always abrupt; there was significant but incomplete cell loss (thinning) that appeared toward the advancing viral front in most wells. Although subjectivity was introduced in the manual outline of the infected area, the variability in area measurements among different operators was about 3–4%, considerably less than the scatter in replicate measurements. The infected area was then approximated as a circle. The radius [$r = (A/3.14)^{1/2}$] of that circle was computed and used as a first approximation to the radial distance of viral spread from the starting point of the focal infection. This r value was designated the area equivalent radius (AER). At each time point during infection 3–12 replicates (average of 6) were performed. The infected areas were measured, and area equivalent radii were calculated and in some cases averaged. The averaged AERs were plotted as a function of time with error reported as standard error of the mean (SEM). Replicates were subjected to an outlier test such that they were rejected if they fell outside 75% of the

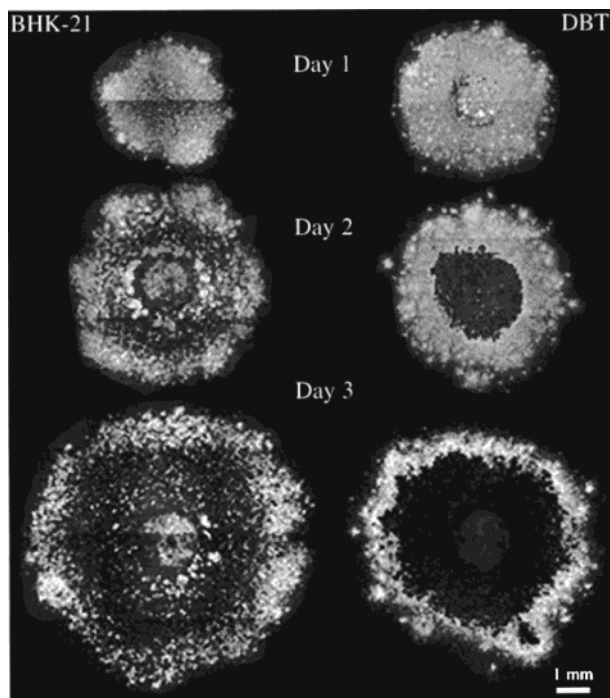


Figure 2. The pattern of VSV infection was distinctly different in BHK-21 cells and DBT cells. The fluorescent micrographs above represent high titer VSV infections of cell monolayers on days 1–3 postinfection. The extent of infection is visualized by immunostaining of VSV-G protein. On day 1, the infection propagated slightly further radially in DBT cells than in BHK-21s. By day 2, the infected area in BHK-21s had increased beyond that of the DBTs. The DBT cells exhibited more complete cell death near the center of the infection, while the BHK-21 cells show more cell loss and thinning. By day 3, the radial spread of both the BHK-21 and DBT infections had increased and more so in the case of the BHK-21 cells. The DBT cells had died and lifted off except in a small ring near the advancing infection front. By day 5 (not shown) the DBT cell death front had caught up to the virus infection front, leaving healthy cells beyond the death perimeter; BHK-21 infection continued.

average value with all replicates included. In this report, fewer than five single measurements from all experiments were omitted using this criterion. To calculate front velocities, raw replicates were plotted and fit to a straight line whose slope yielded the velocity.

Results

VSV spread was distinctly different in BHK-21 and DBT cells, but differences were not apparent by plaque assay. BHK-21 and DBT cells were focally infected with doses ranging from 2.5 up to 2.5×10^6 pfu/well. A parallel plaque assay was also performed. Focally infected cells were fixed and immunostained for the presence of VSV-G protein as an indicator of infection (Figure 2). Cells were also stained with DAPI for death front identification. On day 1, the DBT cells showed a slightly greater infected area than the BHK-21 cells, but this trend slowed and was reversed by day 3. It was also noted that the death of cells in the DBT-infected monolayers proceeded faster and more completely than in the BHK-21 monolayers, which exhibited a marked cytopathic effect, but incomplete cell loss near the advancing virus front.

Figure 3 (top) presents a histogram of average plaque radius as measured by plaque assay at three separate times. At 24 h postinfection no plaques were yet visible in the DBT monolayers. At 36 h there were plaques in both monolayers, and by 48 h they had enlarged. These

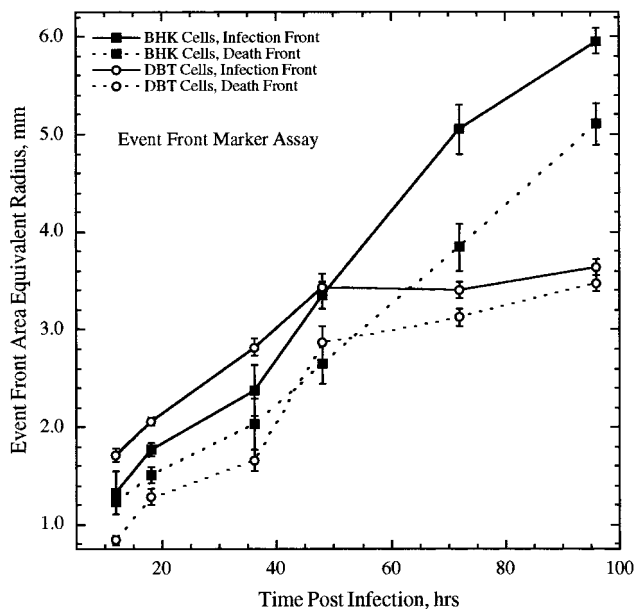
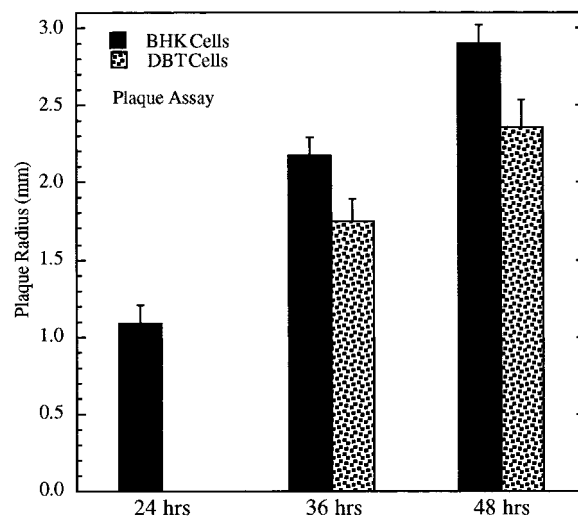


Figure 3. Plaque size increases for BHK-21 and DBT cells presented an incomplete picture of the actual extent of viral spread. The top panel is a comparison of plaque assays in BHK-21 and DBT cells, while the bottom panel is an event front marker assay in the same cell types. The DBT infected area was actually larger than that of BHK-21s up to about 50 h postinfection, as in seen clearly in the bottom panel, while the plaque assay would suggest exactly the opposite. The death fronts, which were comparable to the plaque radii, parallel the infection fronts, with a subtle difference between the two lines. With DBTs the difference between infection and death fronts was initially large but approached zero at long times postinfection. With BHK-21 cells, the difference in radial distance was initially small and increased, reaching a constant value by 50 h. A total of 2.5×10^6 pfu were deposited in the reservoir at the start of the infection in the bottom panel, explaining the presence of a death front by 12 h postinfection. The death fronts exhibited smaller radii overall than the plaques as a result of the higher resolution of the microscopic measurement.

results indicate that VSV propagated faster in BHK-21 cells, as plaques were apparent earlier and they were larger. Otherwise, the behavior could be judged comparable.

With our event front marker method, we were able to visualize newly infected cells well beyond the plaque region. The infected area identified by our method indicated that the infection had proceeded radially nearly twice the distance measured by the plaque assay at the two early time points in both cell lines. The expansion

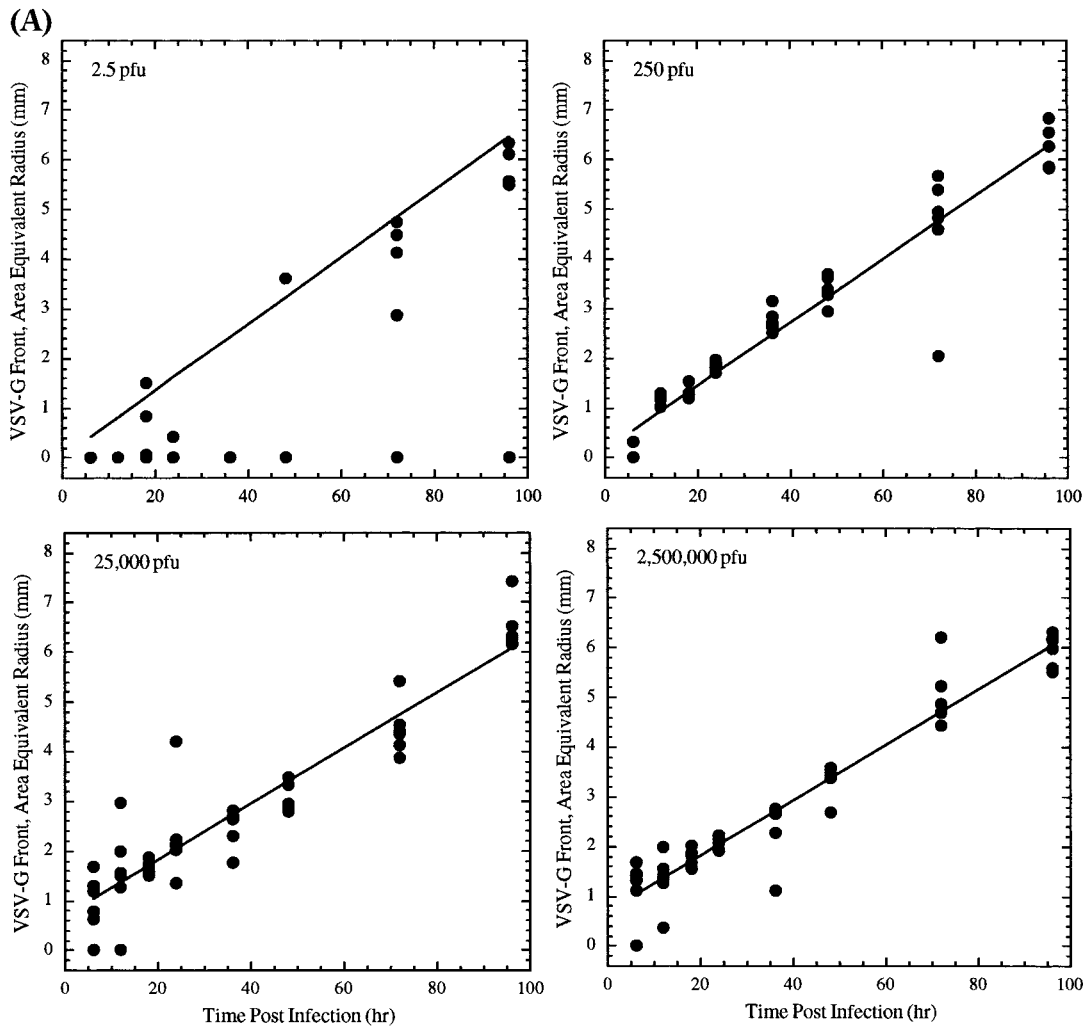


Figure 4. (A) The propagation profile of VSV in BHK-21 cells was relatively insensitive to initial titer. Six replicate monolayers were focally infected at titers ranging from 2.5 to 2.5×10^6 pfu. AER was plotted vs time postinfection for each titer to obtain a viral spread profile. The lines represent a best fit to the raw data as described in the text. Monolayers that did not become infected were excluded from the calculation. To a first approximation, viral spread was linear, with propagation velocities (slopes of the line) ranging from 67 to $56 \mu\text{m/h}$, a variation of 16% over 6 orders of magnitude in initial titer.

outward from the viral reservoir was actually *larger* for the DBT cells than for the BHK-21s at 24 h, although no plaques in the DBT monolayers could be detected by plaque assay. It was also noted that the infection stopped at about 48 h in the DBT cells and the death front had nearly caught up to the infection front by 96 h.

BHK-21s, on the other hand, permitted infection throughout the experiment and, cell death proceeded outward at approximately the same rate after an initial period.

The dependence of VSV spread on initial titer in BHK-21 and DBT cells was very different. Figures 4A and 4B illustrate the effect of initial titer on the propagation profiles of the VSV infection front in the two cell types. Given sufficient virus to initiate infection at all, VSV propagation in BHK-21 cells was relatively insensitive to the initial inoculum placed into the reservoir. The lines drawn through the data (Figure 4A) represent a linear best fit to all of the raw data points, excluding those that did not infect. The lowest titer fit (2.5 pfu/well), in contrast, represents a selection of only the two largest infected areas at the time of fixation. The reason for this selection was our assumption that the smaller area infections probably were not initiated at the same time as the larger ones, as a result of the very low number of infectious virions available. An active virion

most likely had to diffuse from the sides of the reservoir to the monolayer. We cannot rule out, however, the possibility that at very low titer we were sampling some of the lower fitness members of the viral population. The linear fit was a reasonable first approximation to the front velocities, although there were some indications that propagation was not rigorously linear. This is a topic currently under investigation in our laboratory and will be addressed in future studies. For BHK-21, the range of propagation rates varied from $67 \mu\text{m/h}$ at the lowest titer to $56 \mu\text{m/h}$ at the highest (See Table 1.) While these values reflect a slightly decreasing trend with higher initial titer, the differences were not statistically significant. This trend was, however, reproduced in four separate experiments.

The results of infection of the DBT cells was entirely different. At the lower two titers the propagation profiles were very similar to that of the BHK-21 cells, and in fact, the velocity was slightly higher. Using the same exclusion criteria applied to the BHK-21s, the best fit line revealed a propagation velocity of 78 and $76 \mu\text{m/h}$, respectively. As the titer was raised, the infection front advanced less in the same time interval and plateaued earlier. At intermediate titers, more scatter was also noted in the raw data. The propagation velocity for the first 48 h post-infection (or 96 h for the lowest two titers) was approx-

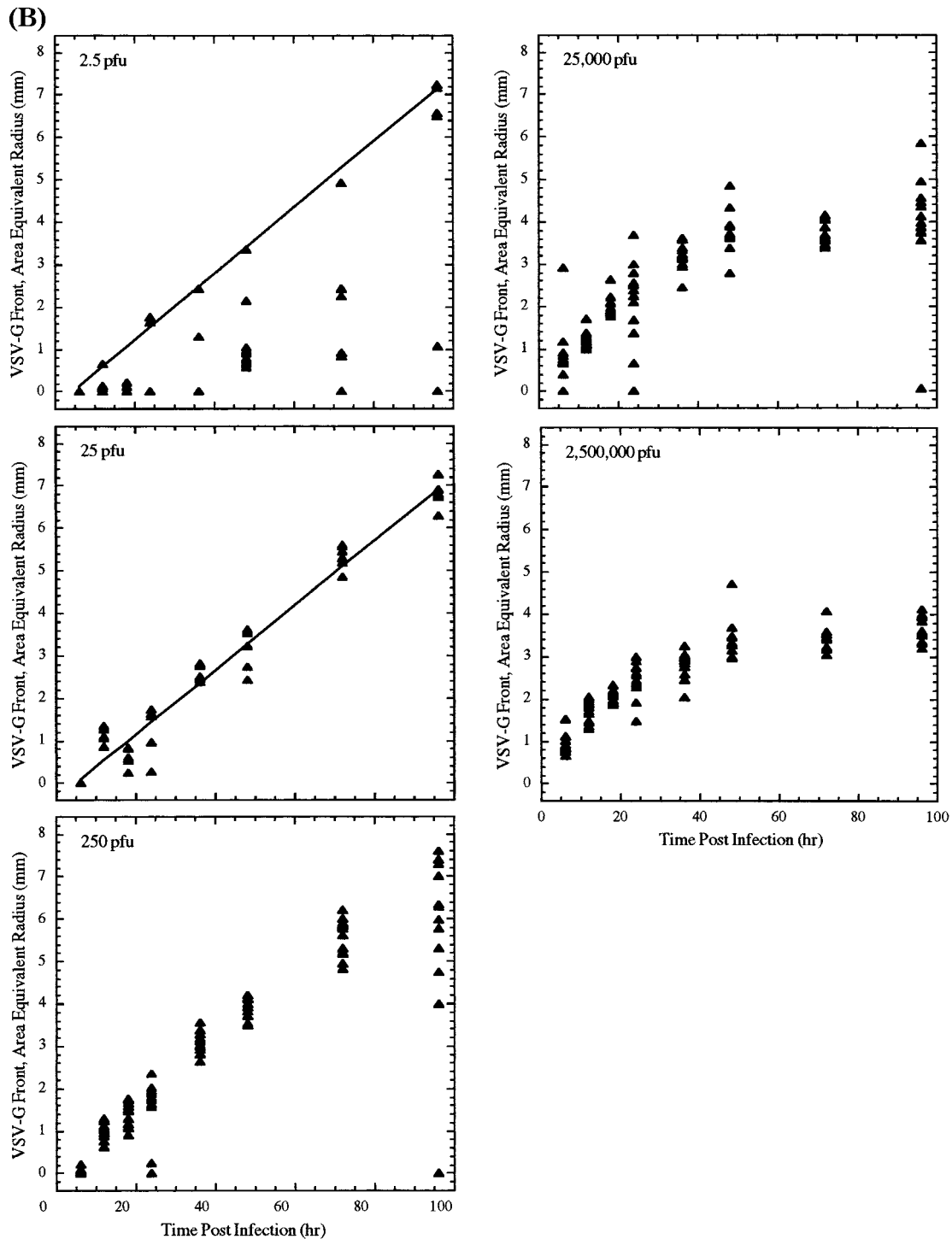


Figure 4. (Continued) (B) VSV propagation profiles in DBT cells were very sensitive to initial titer. Six replicate monolayers were focally infected at titers ranging from 2.5 to 2.5×10^6 pfu. AER was plotted vs time postinfection for each titer to obtain a viral spread profile. Unlike the BHK-21 cells, viral spread was arrested at moderate to high initial titer. The lines for the two lower titers represent a best fit through the two largest infected areas (2.5) and all raw data points (25 pfu), respectively. The first 48 h of the three highest titer infections were approximated as linear in order to make comparisons to the BHK-21 infections (See Table 1). The propagation velocities in these monolayers ranged from 89 to 55 $\mu\text{m}/\text{h}$.

imated as linear to directly compare to the behavior in the BHK-21 system. The slopes varied from 78 $\mu\text{m}/\text{h}$ at the lowest titer, to 55 $\mu\text{m}/\text{h}$ at the highest, again very similar to the BHK-21 case. There were most likely host-based factors that were capable of arresting VSV growth in the DBT cells and were either not present or not effective in the BHK-21 cells. This result is especially interesting, given that both cell lines are permissive for significant VSV replication. Variation, however, was

much larger between highest and lowest velocities, reaching 34%. These initial titer experiments were repeated twice, and both velocities and absolute sizes of infected areas were very reproducible. It should also be noted that the plateau observed at high titer was not due to some nonspecific cytotoxic effect. Parallel infected and noninfected monolayers remained reasonably viable throughout the entire infection (>80% by trypan blue exclusion).

Table 1. VSV Propagation Velocities in BHK-21 and DBT Cells

infection (days postplating)	infectious titer (pfu)	propagation velocity (mm/h)	intercept (mm)	correlation coefficient, R^2
BHK-21				
	2.5×10^0	0.067	0.015	0.98
	2.5×10^2	0.064	0.18	0.92
	2.5×10^4	0.056	0.72	0.87
	2.5×10^6	0.056	0.70	0.93
DBT ^a				
	2.5×10^0	0.078	-0.32	0.99
	2.5×10^1	0.076	-0.35	0.98
	2.5×10^2	0.089	-0.28	0.94
	2.5×10^4	0.070	0.55	0.79
	2.5×10^6	0.055	0.92	0.83
BHK-21				
1	2.5×10^1	0.078	-0.32	0.90
2	2.5×10^1	0.071	-0.60	0.99
3	2.5×10^1	0.065	-0.16	0.92
1	2.5×10^6	0.051	0.81	0.90
2	2.5×10^6	0.064	0.16	0.96
3	2.5×10^6	0.058	0.76	0.89
DBT ^b				
1	2.5×10^1	0.076	-0.37	0.96
2	2.5×10^1	0.060	-0.27	0.89
3	2.5×10^1	0.057	0.15	0.87
1	2.5×10^6	0.054	0.91	0.73
2	2.5×10^6	0.046	0.89	0.90
3	2.5×10^6	0.041	0.95	0.85

^a The lower two titers represent a fit through all time points, otherwise only the first 48 h are used in the fit. ^b Only the first 48 h are used in the fit.

The effect of cell age at the time of infection on VSV spread in vitro was more pronounced in DBT cells than BHK-21 cells, but only at low titer. The effect of cell age at the time of infection of was also probed. Cells were infected on 1, 2, and 3 days postplating. No medium exchange was performed until the day the infection was initiated. In the BHK-21 cell line, the differences in propagation velocity as a function of monolayer age were quite small at either high or low titer (Figure 5 and Table 1). The overall trend with later infection was for slightly slower front propagation rates, most likely attributable to increasing cell densities, which imply growth inhibition and concomitant depletion of ribosomes, metabolite stores, etc. The changes observed, however, were within the range of variability between experiments. With the DBT cells we noted that at high titer the profile differences between the three ages were not significant (Figure 5 and Table 1). The infection reached maximal expansion (2.5–3.5 mm) by about 40 h in all three cases. At low titer, however, there were differences in the maximum area equivalent radii at the time the infection was contained: 5.5 mm for 1-day-old cells, 4.5 mm for 2-day-old cells, and 3.5 mm for 3-day-old cells. Moreover, infections in 1- and 2-day-old cells attained their maximal spread later (approximately 72 h) than the 3-day-old cells (48 h).

Again, effects related to cell density certainly played some role, but that role may have been two-fold. The larger number of cells likely resulted in a slightly slower propagation velocity, but any cell–cell signaling events related to the viral containment may have been facilitated by the small intercellular distances. Until the factor(s) responsible for the containment are identified, it remains unclear whether the differences in propagation profiles were uniquely due to cell density and not also related in some way to the aging of the DBT cells and a concomitant reduction in susceptibility to infection.

The cell age experiments were repeated three times over different time scales and with varying degrees of temporal resolution (3–24 h). Identical trends were observed in each set of experiments. Interpolated time and maximum radius of containment varied by no more than 20% under identical conditions. Preliminary experiments (data not shown) indicated that propagation profiles in DBT cells may be much more sensitive to cell density at plating than those of BHK-21. This consideration is currently under investigation in our laboratory and will be treated in more detail in a future report.

Discussion

This study represents our first effort in developing imaging methods that allow multiple events to be simultaneously probed and quantified. In this set of experiments we established the feasibility of the event front marker assay by examining the effects of initial titer and cell age on VSV propagation. The first two events probed were viral spread and cell death. It should be emphasized that this assay is ultimately intended to monitor the dynamics of infection spread through the monolayer and host responses to that infection. While the propagation rate is obviously related to the viral replication rate, neither our event front marker assay nor the conventional plaque assay is intended as a means to directly quantify viral replication. Factors contributing to the propagation rate include (1) intrinsic viral replication rate, (2) ability of the virus to migrate through the overlay to adjacent cells, (3) mechanism of viral spread, e.g., via budding and diffusion or cell–cell fusion and cytoplasm sharing, and (4) effectiveness of host containment mechanisms. There are better methods for estimating viral replication rates, such as plotting one-step growth curves. Here all cells are infected simultaneously and viral titer is measured at defined time intervals postinfection by plaque assay.

Although conventional plaque assays at the same level of temporal resolution as our method would yield roughly similar trends and have been reported in the literature (23), the majority were done at only one time point. Even at its present level of development, event front markers offer additional information beyond what is obtained by conventional plaque assay. Briefly, a plaque assay works best when the virus is strongly cytolytic, i.e., when the virus rapidly kills the cells leaving a “hole” in the cell monolayer that is visible to the naked eye after fixation and staining with Gentian violet dye. While many viruses are plaque formers, many are not, and therefore infection cannot be detected without the addition of immunostaining. Additionally, our assay permits one to measure the rate of infection spread and cell killing simultaneously, which is an added dimension of information. Moreover, viruses must replicate and spread before any cell death occurs. Our method allows for detection of viral proteins as early as 3 h postinfection with VSV. By plaque assay, one must wait a minimum of 6–12 h before detecting even microscopic plaques and generally 24 h or more for reasonably sized ones. Our assay provides all the information of a plaque assay in the death front and additional information about how much further the virus is propagating in advance of the death front (generally considerably). This information allows one to determine how much time elapses between infection and frank cell death, which cannot be obtained from a plaque assay. Ultimately, our assay will permit other kinds of information to be collected in parallel with viral spread and host death. For example, host markers that are involved in cell–cell signaling or host defense can be detected in

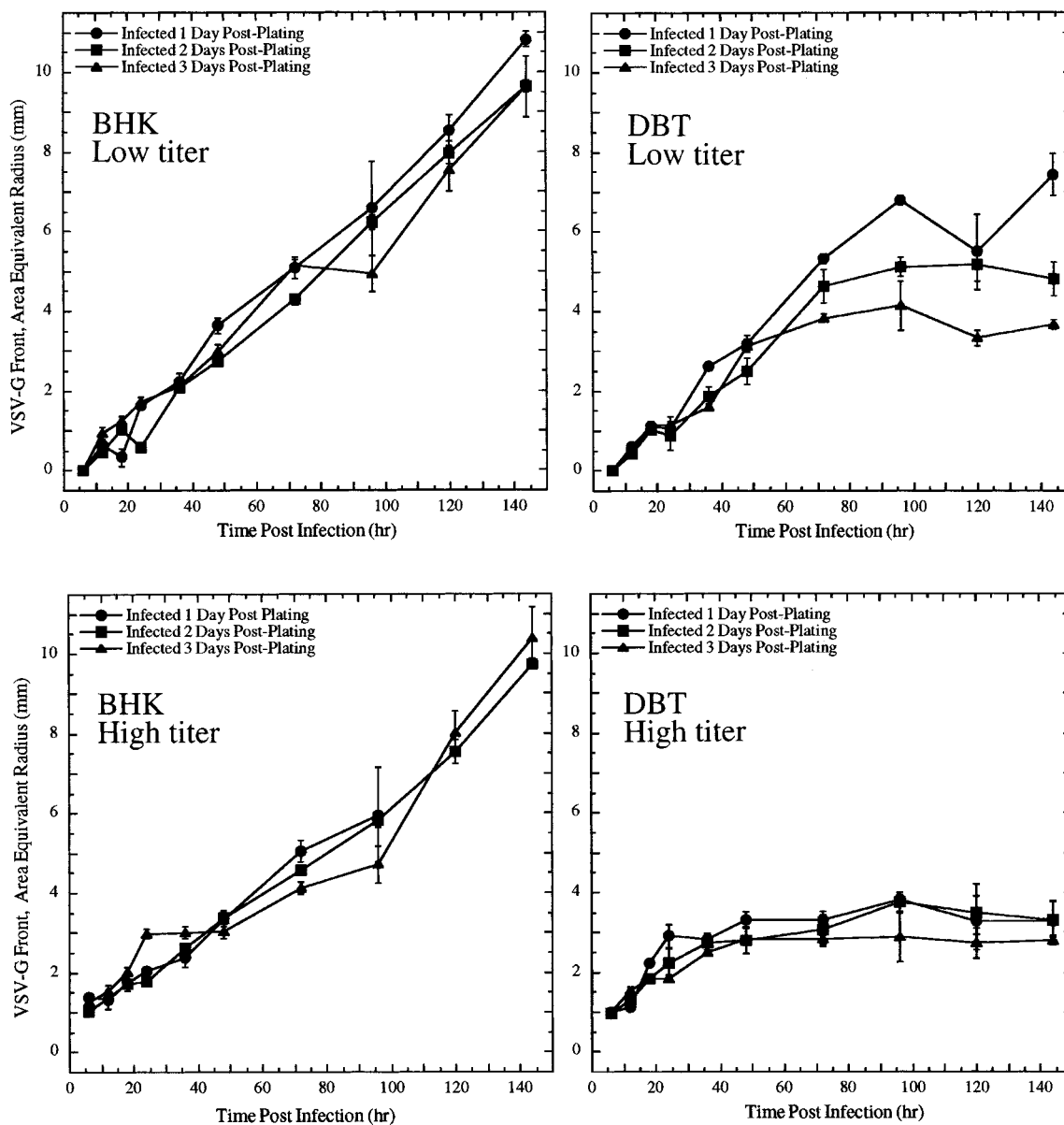


Figure 5. Cell age effects were negligible for BHK-21 and DBT cells at high viral titer. Cells were plated and infected 1, 2, and 3 days postplating to examine the influence of host cell age on propensity to spread. Propagation profiles for BHK-21 cells were similar at high and low titer, regardless of age at the time of infection. Minor differences were most likely attributable to slight variations in cell density. High titer DBT infections followed an identical pattern. Low titer DBT infections, however, exhibit greater variability with respect to both time of containment and maximum spread. Cell density effects probably also contributed here but in two ways; higher density slowed propagation yet accelerated certain types of signaling processes which may have been responsible for containment.

addition to viral proteins in advance or trailing the viral protein front to provide a broader range of dynamic information. Efforts are presently underway in our laboratory to gain additional information about host-based responses in advance of viral spread. As there is often a significant degree of constitutive expression of host-based proteins involved in antiviral defenses, quantification of responses becomes more complex, and measurement of area equivalent radius will not likely suffice.

From a methodological standpoint, quality and consistency of the agarose overlay were the most important variables for success of this assay. Precision within replicates and inter-experiment reproducibility depended on a consistent agarose layer. The ideal scenario was a relatively rigid overlay with minimal microchanneling between the agarose and the cells. We tested several agarose types (high vs low melting, variable purity

grades) from three vendors at concentrations ranging from 0.3% to 2%. All agarose lots were successful, but each required a different percentage of agarose, ranging from 0.6% to 1.0%, to achieve optimal results. In addition, agarose aging resulted in a firmer overlay at lower than normal concentration. In our hands, an older lot of high purity, high melting point Biorad agarose gave very reproducible results at 0.6% using 4 mL overlays. There are basically three reasons that explain these observations: (1) Different percentages of agarose give rise to overlays of very different viscosity, thereby changing the diffusion rate of the virus through the overlay. (2) The extent of branching and cross linking between polymers in agarose from different sources varies, resulting in different migration rates. (3) Different types of agarose have various kinds of impurities, some of which may deleteriously affect either host cells or budding virions.

If cell health is compromised, the host may not support viral replication well. Certain impurities are capable of inactivating viruses, thereby slowing the spread. It is therefore very important that experiments to be directly compared be conducted under identical experimental conditions with respect to the overlay.

The effect of initial titer in the reservoir was an interesting one. In BHK-21 cells that failed to arrest VSV spread, titers ranging over several orders of magnitude resulted in very similar, roughly linear, propagation profiles. The hypothesis was that expansion of the VSV-G front depended primarily on the replication rate of the virus within that host. Presumably, infected BHK-21 cells did not signal uninfected cells to prepare to resist the viral challenge, and if they did, the signals were not effectively transduced. The DBT behavior, on the other hand, was very striking. In this assay approximately 4,000 cells (the number of cells estimated to be present in the reservoir) may be simultaneously infected. The fact that the infection was contained suggests that there may be a signaling event, such as the production of interferon, that was initiated very early in the infection process. We speculate that there was some critical threshold for "signal activation". When a very small number of cells was infected, there was not enough signal generated to produce the inhibitory effect, and we observed behavior very similar to that of the BHK-21 cells even very late in infection. As the titer was increased, we noted that there seemed to be more scatter in the data at the later time points, indicating that in some cases the threshold was met and in others, it was not. As we moved to high titer, the arrest of infection spread was very fast and complete; signal propagation was effective in all cases. In this case, most likely all 4,000 cells were multiply infected at the outset of the experiment. There are, however, other possible explanations for this behavior. One would be that the cells were damaged and/or dying when the propagation was arrested. This is clearly not the case, as we have ascertained that cell viability was reasonably high (>80%) even at the later time points for both infected and uninfected DBT monolayers. A large excess of defective interfering particles could be responsible for this phenomenon, but it then becomes hard to explain why the BHK-21 cells do not exhibit the same behavior under any circumstances. Future experiments can measure the possible participation of interferon in this assay by using cells from transgenic mice deficient in interferon receptors or by using anti-interferon serum in the infection medium. Experiments currently underway in our laboratory suggest that NO synthesis is required for arresting VSV spread, and results from these studies will be treated in detail in a future report describing the extension of the method to host event markers.

Effects due to cell age at the time of infection were minimal and unsurprising. Propagation velocities for BHK-21 cells were similar, independent of cell aging. Minor differences were most likely attributable to slight variations in cell density. In addition to the larger number of cells that must be infected, higher cell density implies growth inhibition and concomitant depletion of ribosomes and other resources needed for viral replication. High titer DBT infections followed an identical pattern as the BHK-21s. Low titer DBT infections, however, exhibit greater variability with respect to both time of containment and maximum spread. Cell density effects probably also contributed here but in two ways: higher density slowed propagation yet may have accelerated certain types of signaling processes responsible for con-

tainment of the infection. Preliminary experiments (data not shown) suggest that low cell density may prevent the containment of infection observed with high initial titers, but more work is required to validate this result.

In summary, our event front marker assay is robust when performed under identical conditions and yields quantitative propagation profiles in vitro. Moreover, the method provides information that might be missed in traditional plaque assays and can be extended to include cell-based antiviral responses that underlie differences in propagation profiles. We hope that our method may find applications as (1) a prescreening system for novel antiviral therapeutics targeting any phase of the viral life cycle, (2) a reporter system for synergistic cytopathological effects arising from virus–drug interactions, and (3) a fundamental kinetic probe of the complex dynamics of virus/host and infected/uninfected cell interactions for eventual in silico simulations.

Acknowledgment

The authors gratefully acknowledge technical assistance provided by L. Belinski, E. Keller, H. Lewison, J. Ramacher, and B. Rittenhouse. They also wish to thank P. Mathews (NKI/NYU) for providing the IL-2 anti-VSV-G antibody. This work was supported by a Whitaker Foundation Biomedical Engineering Research Grant (award 0087939), the National Institutes of Health Research Service Award 5T32 GM08349 from the NIGMS (V.L.), and a National Science Foundation Graduate Fellowship (E.E.E.).

References and Notes

- Duggin, D. J.; Bittner, M.; Chen, Y. et al. Analysis of Gene Expression Microarrays for Phenotype Classification. *Nature* **1999**, *21*, 10–14.
- Califano, A.; Stolovitzky, G.; Tu, Y. Analysis of Gene Expression Microarrays for Phenotype Classification. *Proc. Int. Conf. Intell. Syst. Mol. Biol.* **2000**, *8*, 75–85.
- Celis, J. E.; Celis, P.; Ostergaard, M. et al. Proteomics and Immunohistochemistry Define Some of the Steps Involved in the Squamous Differentiation of the Bladder Transitional Epithelium: A Novel Strategy for Identifying Metaplastic Lesions. *Cancer* **1999**, *9*, 3003–3009.
- Holstege, F. C. P.; Jennings, E. G.; Wyrick, J. J. et al. Dissecting the Regulatory Circuitry of a Eukaryotic Genome. *Cell* **1998**, *95*, 717–728.
- Cummings, C. A.; Relman, D. A. Using DNA Microarrays to Study Host–Microbe Interactions. *Emer. Infect. Dis.* **2000**, *6*(5), 513–525.
- Iyer, V. R.; Eisen, M. B.; Ross, D. T. et al. The Transcriptional Program in the Response of Human Fibroblasts to Serum. *Science* **1999**, *283*, 83–87.
- Haller, A. A.; Nguyen, J. H.; Semler, B. L. Minimum Internal Ribosome Entry Site Required for Poliovirus Infectivity. *J. Virol.* **1993**, *67*(12), 7461–7471.
- Laille, M.; Gerald, F.; Debitus, C. In Vitro Antiviral Activity on Dengue Virus of Marine Natural Products. *Cell Mol. Life Sci.* **1998**, *54*(2), 167–170.
- Appleyard, G.; Maber, H. B. Plaque Formation by Influenza Viruses in the Presence of Trypsin. *J. Gen. Virol.* **1974**, *25*(3), 351–357.
- Appleyard, G.; Maber, H. B. A Plaque Assay for the Study of Influenza Virus Inhibitors. *J. Antimicrob. Chemother.* **1975**, *1*(4), 49–53.
- Wengler, G. Comparative Studies on Polyribosomal, Non-polyribosome-Associated and Viral 42S RNA from BHK 21 Cells Infected with Semliki Forest virus. *Virology* **1975**, *65*(2), 601–605.
- Zavada, J.; Zazadova, Z.; Malir, A. et al. VSV Pseudotype Produced in Cell Line Derived from Human Mammary Carcinoma. *Nat. New. Biol.* **1972**, *240*(99), 124–125.

- (13) Tobita, K.; Sugiura, A.; Enomote, C. et al. Plaque Assay and Primary Isolation of Influenza A Viruses in an Established Line of Canine Kidney Cells (MDCK) in the Presence of Trypsin. *Med. Microbiol. Immunol.* **1975**, *162*(1), 9–14.
- (14) Cave, D. R.; Hendrickson, F. M.; Huang, A. S. Defective Interfering Virus Particles Modulate Virulence. *J. Virol.* **1985**, *55*(2), 366–73.
- (15) Francoeur, A. M.; Poliquin, L.; Stanners, C. P. The Isolation of Interferon-Inducing Mutants of Vesicular Stomatitis Virus with Altered Viral P Function for the Inhibition of Total Protein Synthesis. *Virology* **1987**, *160*(1), 236–245.
- (16) Cantell, K.; Paucker, K. Studies on Viral Interference in Two Lines of HeLa Cells. *Virology* **1963**, *19*, 81–87.
- (17) Francoeur, A. M.; Lam, T.; Stanners, C. P. PIF, a Highly Sensitive Plaque Assay for the Induction of Interferon. *Virology* **1980**, *105*, 526–536.
- (18) Lee, Y.; Yin, J. Detection of Evolving Viruses. *Nat. Biotechnol.* **1996**, *14*(4), 491–493.
- (19) Letchworth, G. J.; Rodriguez, L. L.; del Barrera, J. Vesicular Stomatitis. *Vet. J.* **1999**, *157*, 239–260.
- (20) Holland, J. J.; Villarreal, L. P.; Breindl, M. Factors Involved in the Generation and Replication of Rhabdovirus Defective T Particles. *J. Virol.* **1976**, *17*(3), 805–815.
- (21) Ball, L. A.; Pringle, C. R.; Flanagan, B. et al. Phenotypic Consequences of Rearranging the P, M, and G Genes of Vesicular Stomatitis Virus. *J. Virol.* **1999**, *73*(6), 4705–4712.
- (22) Lefrancois, L.; Lyles, D. S. Antigenic Determinants of Vesicular Stomatitis Virus: Analysis with Antigenic Variants. *J. Immunol.* **1983**, *130*, 394–398.
- (23) Stanners, C. P.; Francoeur, A. M.; Lam, T. Analysis of VSV Mutant with Attenuated Cytopathogenicity: Mutation in Viral Function, P, for Inhibition of Protein Synthesis. *Cell* **1997**, *11*, 273–281.

Accepted for publication September 17, 2001.

BP010115M